Reducing and multiple-element doping of graphene oxide using active screen plasma treatments

Chen, Jian; Shi, Xiangru; Qi, Shaojun; Mohai, Miklós; Bertóti, Imre; Gao, Ying; Dong, Hanshan

DOI:
10.1016/j.carbon.2015.08.046

Accepted Manuscript

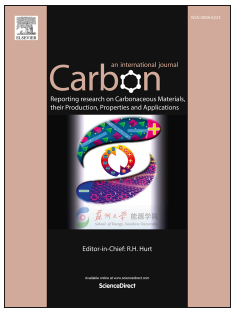

Reducing and multiple-element doping of graphene oxide using active screen plasma treatments

Jian Chen, Xiangru Shi, Shaojun Qi, Miklós Mohai, Imre Bertóti, Ying Gao, Hanshan Dong

PII: S0008-6223(15)30164-0

DOI: 10.1016/j.carbon.2015.08.046

Reference: CARBON 10211

To appear in: *Carbon*

Received Date: 29 March 2015

Revised Date: 25 July 2015

Accepted Date: 15 August 2015

Please cite this article as: J. Chen, X. Shi, S. Qi, M. Mohai, I. Bertóti, Y. Gao, H. Dong, Reducing and multiple-element doping of graphene oxide using active screen plasma treatments, *Carbon* (2015), doi: 10.1016/j.carbon.2015.08.046.

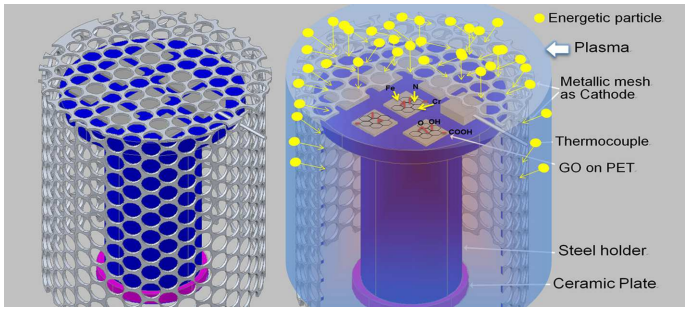

Reducing and multiple-element doping of graphene oxide using active screen plasma treatments

Jian Chen*‡[a], Xiangru Shi[a], Shaojun Qi[b], Miklós Mohai[c], Imre Bertóti‡[c], Ying Gao[a], Hanshan Dong‡[b]

[a] Jiangsu Key Laboratory of Advanced Metallic Materials, School of Materials Science and Engineering, Southeast University, Nanjing 211189, China.

[b] School of Metallurgy and Materials, The University of Birmingham, Birmingham, B15 2TT, UK

[c] Institute of Materials and Environmental Chemistry, Research Centre for Natural Sciences, Hungarian Academy of Sciences, Budapest, H-1519 Hungary

‡ These authors contributed equally to this work.

*Corresponding author: Tel/Fax: 86 25 5209-1090, E-mail: j.chen@seu.edu.cn (Jian Chen)

Abstract

A transparent graphene oxide layer on a non-conductive poly (ethylene terephthalate) film was treated by a new active screen plasma technology at temperatures ranging from 100ºC to 200ºC in pure hydrogen and in a gas mixture of hydrogen and nitrogen. To study the thermal reducing effects of the active screen plasma, parallel thermal annealing treatments were also carried out at the same temperatures. UV-visible absorption spectra, X-ray diffraction, Raman spectroscopy, X-ray photoelectron spectroscopy (XPS) and electrical properties confirmed that the graphene oxide can be effectively reduced by the active screen plasma treatments. Detailed XPS quantitative analyses have revealed that the carboxylic groups are not stable, and their amount can be decreased effectively by the active screen plasma treatments. Only about one third of the carbonyl type C=O can be reduced at the same time. In addition to the reduction, simultaneous multi-element doping of GO with nitrogen from the gas supply and with Fe, Cr and Mo from the stainless steel active screen was also detected by XPS.

1. Introduction

Graphene has received significant attentions in the past years due to its excellent charge carrier mobility, thermal conductivity, optical transparency and mechanical properties.[1, 2] Various synthesis methods [3-5] have been proposed to obtain high-quality graphene with large-size and/or large quantity. Among these methods, the chemical solution route through the precursor graphene oxide (GO) gained great successes as it enables the massive production and the chemical functionalization of graphene.

GO has a similar sheet-like structure as graphene and each GO nano-sheet can be considered as a multifunctional network.[6, 7] It contains several oxygen functionalities including hydroxyls, epoxides, diols, ketones and carboxyls, which are attached to the carbon backbone. The reduced GO (rGO) can then be obtained by removing the oxygen functionalities to recover the physical properties of graphene. A diversity of reducing methods[8] have been developed such as chemical agent reaction,[9] thermal annealing,[10] microwave irradiation,[11] photocatalysis,[12] electrochemical reaction,[13] and solvothermal reduction.[14] The most widely used methods are the chemical agent reaction and the thermal annealing.

Chemical reagent reduction, involving hydrazine,[9, 15-17] metal hydrides,[18] alkaline (NaOH),[19] ascorbic acid (Vitamin C)[20, 21] and hydroiodic acid (HI),[22] etc., is based on their chemical reactions with GO. Although large quantities of rGO can be obtained due to the facile solution-based reduction, these chemical agents are usually hazardous and sometimes harmful to the support for the graphene and the environment. On the other hand, thermal annealing is effective in reducing GO,[10, 15, 17, 23-26] and the reduction extent can be improved with the increase of the temperature. But its drawbacks are also obvious as heating requires large energy consumption and critical conditions.[8] Moreover, GO on the substrates with low-melting points, such as polymers for flexible electronic devices, cannot be effectively reduced without substrate degradation.

Plasma treatments provide one promising option to circumvent these problems, as an eco-friendly and energy-saving alternative to existing processes. Gomez-Navarro *et al*. [6] successfully reduced GO by hydrogen (H_2) plasma, further investigated its atomic scale features. The plasma reduced GO layers were found to comprise of defect-free graphene areas with sizes of a few nanometres interspersed with defective areas dominated by clustered pentagons and heptagons. Wang *et al.* [27] realized reducing and nitrogen doping (N-doping) of GO by a plasma treatment. In another study, GO powders were simultaneously reduced and N-doped at near room temperature by employing a plasma-assisted microwave technology.[28]

It is known that doping is a common strategy in tuning the properties of carbon-based nanomaterial. The doping methods for this two-dimension material are different from the conventional methods for bulk materials. Doping of graphene is a key issue to its future applications, [29] e.g., in field effect transistors, super-capacitors, and lithium batteries because it can confer new chemistry and physics to graphene. For example, N-doping can tune the chemically derived functionalized graphene from being a p-type to n-type semiconductor. Plasma treatments have proven its feasibility in doping graphene. Bertóti *et al*.[30] reported that 15 at.% nitrogen (N_2) was implanted into the graphene surface using a radio frequency activated low pressure N_2 plasma. N-doped graphene was also obtained by exposing thermally reduced GO/glassy carbon to N_2 plasma by Shao *et al*.[31] It was found that N-doped graphene exhibited a much higher electrocatalytic activity toward H_2O_2 reduction than graphene, and a much higher durability and selectivity than the widely-used expensive Pt. Wang *et al*. [27] also obtained N-doped graphene with different percentage (from 0.11 to 1.35 at.%) of N in N_2 plasma by controlling the exposure time.

Notwithstanding the fact that these plasma treatments demonstrated their successes in doping and reducing, they required a conductive electrode such as glassy carbon,[27, 31] or pre-reducing to recover the conductivity,[32] which has eliminated or at least retarded the applications of graphene on non-conductive substrates such as for transparent and flexible graphene-based

electronic devices; in addition, all these plasma treatments can, to date, dope graphene only by nitrogen but multi-element doping is desirable for multi-functionalizing graphene.

A new type of plasma activation, active screen (AS) plasma technology, has been developed in the past few years to overcome the drawbacks of traditional direct current (DC) glow discharge plasma treatments, such as arcing, hollow cathode and edge effects.[33-36] In an AS treatment, the worktable (or the sample) is not the cathode as used in DC treatments but a metallic mesh surrounding the samples and the worktable is serving as cathode. Glow discharge, therefore, does not take place on the surface of the samples and the worktable but on the metal mesh cylinder called as the active screen. The drawbacks of tradition DC plasma can be overcome, furthermore nonconductive materials, such as polymers,[33] biomaterials,[37] can be treated in the AS plasma. Currently, there is still argument on the mechanisms on the AS plasma due to various plasma surface interactions. It has been generally accepted that a mechanism of sputtering and redeposition is of fundamental importance.[38] This could allow for tailoring the surface chemical compositions and physical properties of carbon-based materials by changing two facile parameters, the plasma gas composition and the screen material.

Therefore, it might be feasible to combine the reducing, N-doping and possibly the metallic atoms-doping (from the metallic mesh) of GO on a transparent nonconductive polymeric substrate in one process. In this study, the feasibility of reducing and multi-element doping the GO on a non-conductive poly(ethylene terephthalate) (PET) substrate has been investigated for the first time using the advanced active screen plasma technology. Parallel heat treatments were also carried out to differentiate the plasma effects from the thermal effects. Detailed chemical analysis was carried out using XPS and Raman to study the mechanisms involved in reducing and multi-element doping of graphene.

2. Experimental

2.1 Preparation of GO and GO/PET films

The graphene oxide was prepared at Southeast University using the modified Hummer's method.[39] Natural graphite powder with an average size of 30 μm (1g), $NaNO_3$ (1g) and KMnO4 (6g) were slowly added to H_2SO_4 (230ml) at 0°C (ice bath). Then the mixture was stirred at 0°C for 2hrs and then at 36°C for 2hrs. The solution was then slowly dropped into icy distilled water (230ml) to obtain a graphite oxide suspension. It was further treated with H_2O_2 to reduce the residual permanganate and manganese dioxide, washed with deionized water and centrifuged to completely remove residual salts and acids. The dispersion was ultrasonically treated for 15 min to exfoliate the GO nanosheets. Finally, the GO/PET film samples were prepared by drop casting the dispersion (600 μl) with a GO concentration of 0.25 mg/ml on a rectangle PET substrate (Lumirror T60, Toray Industries, Inc., Japan) with a size of 20x20 mm, and a thickness of 188 μm. These film samples were then dried at 60 ºC. The thickness of the GO layer is measured to be about 20 μm.

2.2 *Active screen plasma treatment*

Active screen plasma treatments were carried out at University of Birmingham using a lab scale active-screen plasma device within a traditional plasma nitriding unit (40 kW Klöckner DC plasma unit). The plasma is formed on the screen made from a stainless steel mesh with the size of holes about 8 mm that acts as cathode and the wall of the chamber is the anode. As the table is isolated from the chamber, the GO/PET samples remain in a floating potential as shown in Figure 1. The sample-mesh distance (from the top of mesh to the table) is about 2.5 cm.

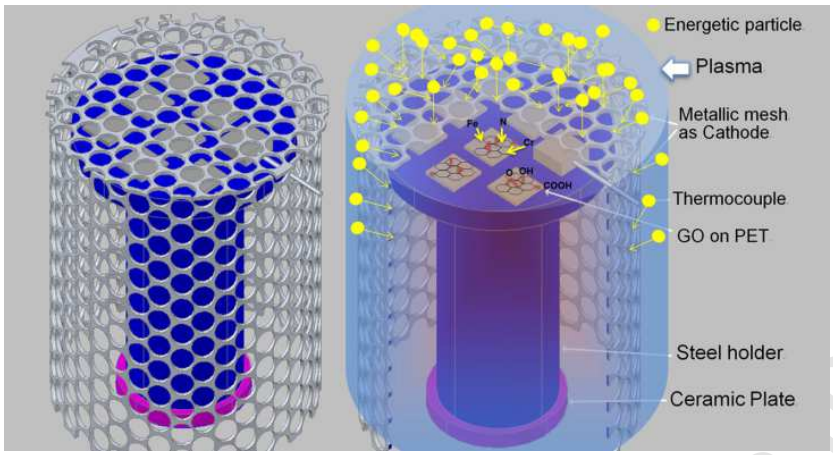

Figure 1. Schematics of active screen plasma treatments

As listed in Table 1, two types of active screen plasma treatments were carried out: (i) in pure H_2 (the ASP series) and (ii) in a gas mixture of 75%H_2 and 25% N_2 (the ASPN series). To differentiate plasma effects from temperature effects, some samples were also heat-treated in pure H_2 using a vacuum furnace (the HT series). The treatments were carried out at temperatures ranging from 100ºC to 200ºC (which is below the melting point of the PET substrate) for 1 hour at a pressure of 400Pa (4mbar). In the following text, these treated samples were named according to their code (Table 1).

Table 1. Sample code and treatment conditions

Sample Code	Treatment	Gas composition	Temperature (°C)
GO	As-cast/untreated	N/A	N/A
HT100	Thermal annealing	100%H_2	100
HT200	Thermal annealing	100%H_2	200
ASP100	AS plasma treatment	100%H_2	100
ASP150	AS plasma treatment	100%H_2	150
ASP200	AS plasma treatment	100%H_2	200
ASPN100	AS plasma treatment	25%N_2+75%H_2	100
ASPN150	AS plasma treatment	25%N_2+75%H_2	150
ASPN200	AS plasma treatment	25%N_2+75%H_2	200

2.3 Characterisation

The prepared GO dispersion was characterized using optical microscope (OM, MV5000, Jiangnan Noval Optical Co., China) and transmission electron microscope (Tecnai G2-T20, FEI Co., USA). The OM and TEM samples were prepared by dissolving a small amount of dispersion in ethanol, and then one droplet was spread over a silicon wafer and copper mesh with carbon film. After dried in the ambient condition, the samples were investigated.

The transparency of as-cast and treated GO/PET samples was characterized using ultraviolet–visible spectroscopy (UV-vis, UV-6000, Shanghai metash instruments Co., China). X-ray diffraction (XRD) was conducted using a D8-Discover X-ray spectrometer (Bruker Co., German), with a Cu Kα radiation. Raman analysis was also carried out (LabRAM HR800, Horiba Jobin Yvon, Japan) using an excitation wavelength of 514.5 nm. Two edges of the graphene/PET samples were coated with silver with a distance about 13 mm, and the electrical conductivity was measured.

Detailed chemical analysis was performed by X-ray photoelectron spectroscopy (XPS). Spectra were recorded on a Kratos XSAM 800 spectrometer, operated at fixed analyser transmission (FAT) mode using Mg $K\alpha_{1,2}$ (1253.6 eV) excitation. The pressure of the analysis chamber was lower than $1 \cdot 10^{-7}$ Pa. Wide scan spectra were recorded for all samples in the 100–1300 eV kinetic energy range using 80 eV pass-energy, with 0.5 eV step and 0.5 s dwell time. High-resolution spectra of photoelectron lines of the main constituent elements of the carbon-containing layers and contaminations were recorded at 40 eV pass-energy by 0.1 eV step and minimum 1 s dwell time. The charge-referencing was made setting the maximum of the C1s to 284.6±0.2 eV. At this referencing, the two types of C–C bonds usually found in graphene type carbon materials are at the most accepted energy. The position for aromatic $C–C_{ar}$ (sp^2) at 284.3±0.2 eV coincides with the most accepted literature data [40, 41], generally applied also by the authors [42, 43], for the undisturbed graphene and the GO. The 'amorphous' $C–C_a$ (sp^3) carbon is located at 285.0±0.2 eV [40, 41, 44-47]. The chemical states of the constituent elements

were determined or assigned according to the available references.[44-47] Quantitative analysis, based on peak area intensities (after removal of the Shirley-type background), was performed by the Vision 2 and XPS MultiQuant programs [48, 49] applying experimentally determined photo-ionization cross-section data of Evans *et al*. [50] and asymmetry parameters of Reilman *et al*.[51]

3. Results and Discussion

3.1 Morphology of prepared GO

For the OM assessments, the GO dispersion was spread over a silicon wafer and it was found that their sizes were similar, ~2 μm as indicated by arrows in Figure 2a. Further TEM analysis was carried out and the results are shown in Figure 2b. The deposited GO nanosheets showed a smooth and flat appearance and there were some wrinkles on the nanosheets since the 2D structure becomes more thermodynamically stable by bending and the functional groups and defects distort the flat graphene plane. The selected-area electron diffraction (SAED) of the GO flakes revealed the multi spot patterns implying that the GO flakes are not monolayered but multi-layered. [52] By measuring the thickness of the wrinkles, the number of the atomic monolayers was calculated to be around 4 for the majority of the GO flakes, assuming the thickness of GO monolayer is 0.8 nm. [53]

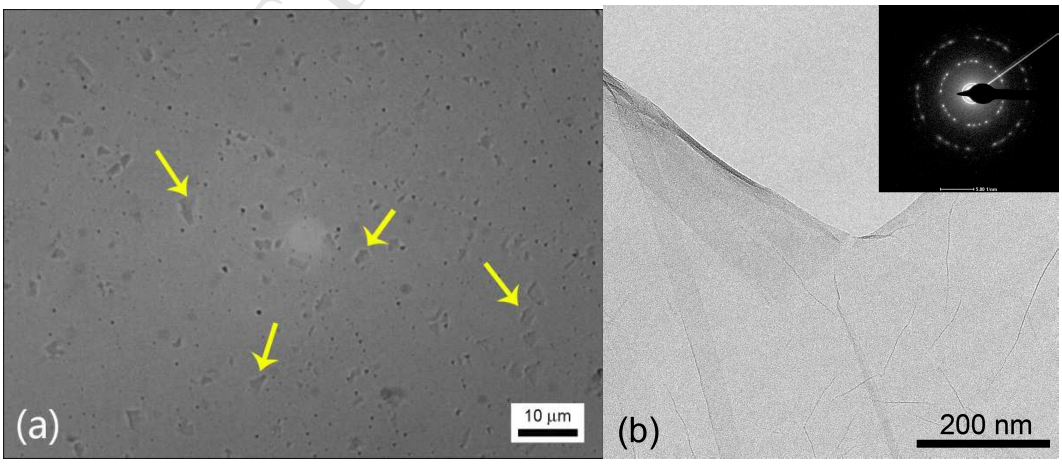

Figure 2. (a) Optical analysis and (b) TEM image of as-deposited GO with insert of the selected area electron diffraction pattern

3.2 Transparency

The as-received PET film (PET-AR) showed a high transparency as shown in Figure 3. The GO/PET sample showed a light brown color and good transparency, ~80% at wavelength 800nm. After ASP and ASPN treatments, the color of the GO/PET samples changed to light silver grey, suggesting that the samples were reduced and part of the graphene conductivity was recovered due to the mobility of electrons.[8] With the increase of the treating temperature, the transmission was decreased for both ASP and ASPN treatments, suggesting the higher temperature can reduce the GO more effectively. It is also noticed that that the transmission for ASP samples was less than that of ASPN samples.

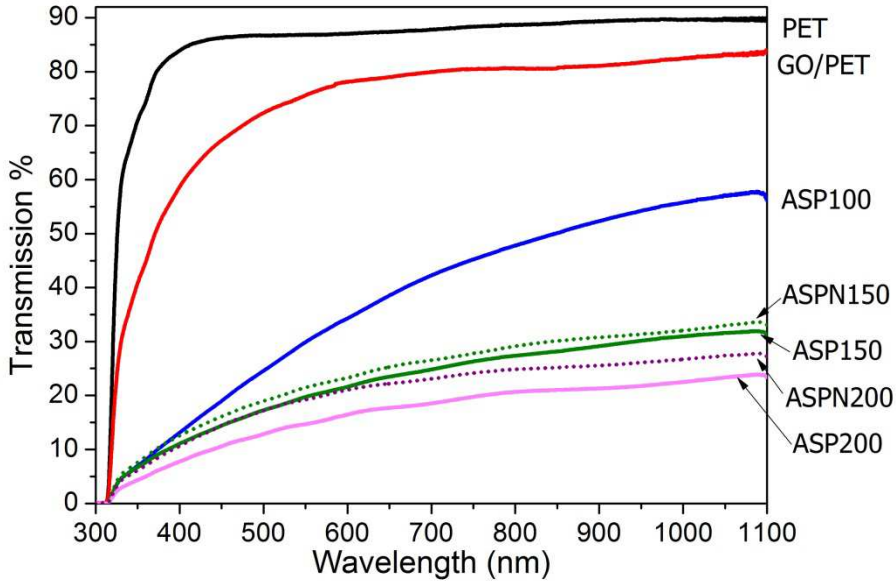

Figure 3. UV-vis results of the PET, GO/PET and the plasma treated samples

3.3 Electrical properties

The electrical resistance of the samples, as shown in Figure 4, significantly decreased with the increase of temperature of the different treatments. For the ASP/ASPN processes, the resistance decreased from 12.6 MΩ to 50 kΩ. It was also noticed that the ASP treated samples consistently showed lower resistance than the HT samples, and the ASPN treated samples exhibited the lowest

resistance. These results indicated that the temperature is not the only dominant factor. The plasma and gas composition can effectively tune the reducing extent of GO materials. To clarify these, further detailed chemical analysis was carried out.

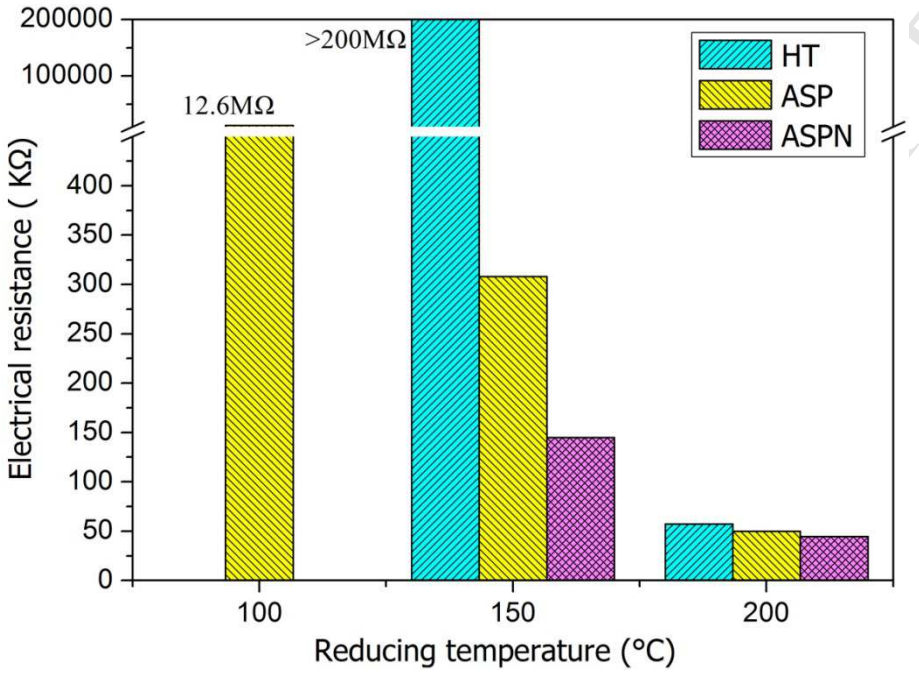

Figure 4. Electrical resistances of the treated samples

3.4 XRD results

XRD patterns showed that the peaks for PET are at 17.7º, 23.0º, 26.0º and 29.4º which also appeared for all GO/PET samples in Figure 5a. However, there is a GO peak at 11.2º for the GO/PET film in Figure 5b. After the ASP100 treatment, this peak shifted to the slightly higher angle and became broader. With the further increase of the temperature, this peak disappeared suggesting that the reduction was more efficient at the higher temperature. In comparison of the different processes at 200 ºC, the HT200, ASP200 and ASPN200 samples showed the similar XRD patterns.

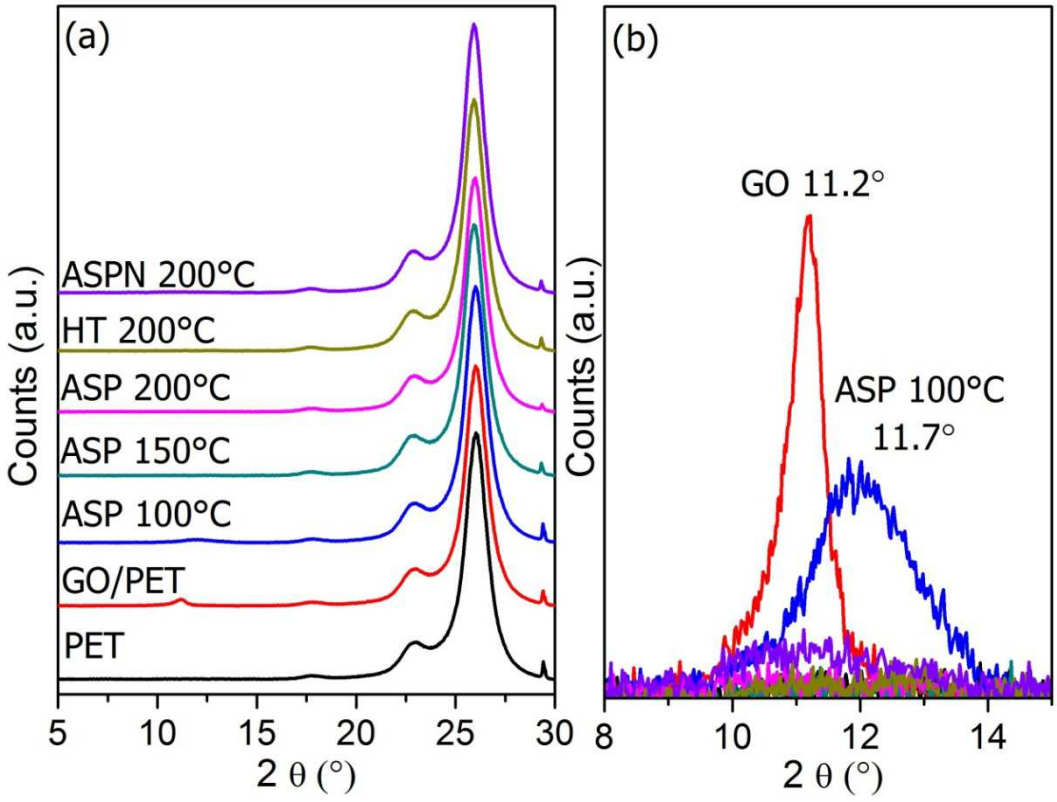

Figure 5. XRD spectra of the PET, GO/PET and the treated samples

3.5 Raman results

The Raman spectrum for as-cast GO in Figure 6 contains two broad G and D bands and two low intensity 2D and D+G bands, similar to the result reported in reference.[54] For the plasma treated samples, the G and D bands exhibit the similar characteristics to those of the as-cast GO, while the 2D and D+G bands are too weak to be identified. It is known [25, 55] that the G band is related to the vibration of sp^2-hybridized carbon, and the prominent D band corresponds to the structural imperfections created partly by the attachment of oxygen, hydroxyl and epoxide groups to the carbon backbone. The area under the D band was integrated from 1250 to 1450 cm^{-1} and that under the G band was integrated from 1500 to 1650 cm^{-1} as demonstrated in Figure 6, and the area ratio of D/G is shown in the parenthesis for each spectrum. It can be seen that the ratio was increased after all plasma treatments, similar to references.[9, 25, 56] This can be attributed to the formation of a number of defects at the surface

of GO during reduction. The G band for ASPN at 200 ºC even showed slightly blue shift which was attributed to a graphitic 'self-healing' by Kudin *et al*.[57] It suggested that GO was possibly reduced more effectively at the high temperature and the assistance of N in the plasma treatments.

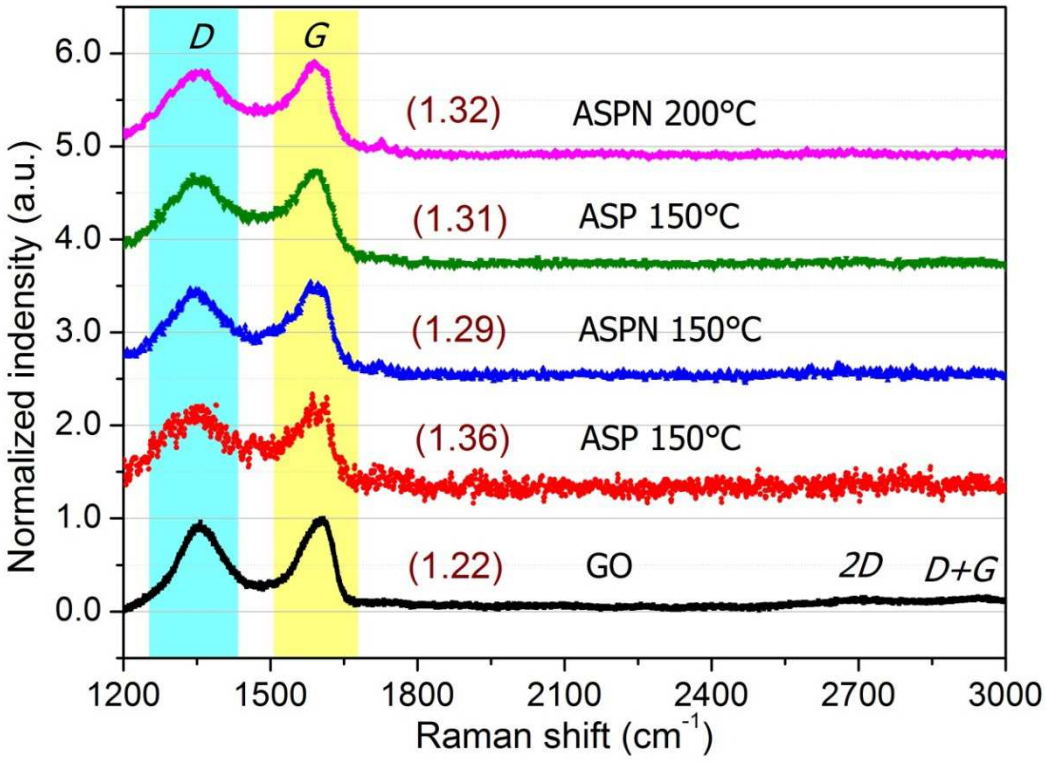

Figure 6. Normalized Raman spectra of the GO and the plasma treated samples with the area ratio D/G being provided in parenthesis

3.6 Composition and chemical states determined by XPS

The survey photoelectron spectra of the untreated and all treated GO layers on the PET substrates were recorded and are shown in Figure 7. In addition to the expected carbon and oxygen, the untreated and the heat treated samples show the presence of oxidized Si contamination. Si was also detected in all other treated samples and thus Si may be originated from the raw graphite powder. After the plasma treatments, elements such as N, Fe, Cr, Mo (and negligible amount of S) were identified on the surface of the samples.

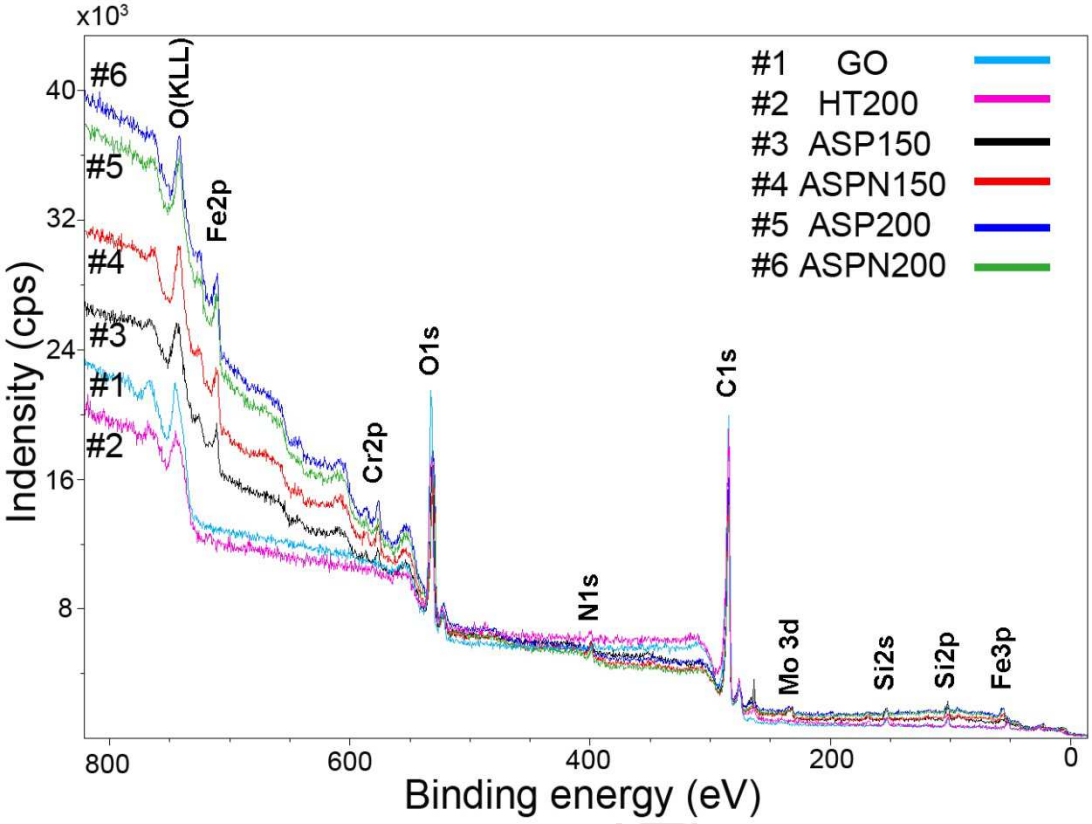

Figure 7. Survey XP spectra of the GO, HT200, ASP150, ASPN150, ASP200 and ASPN200 samples

High resolution spectra were recorded for the major O1s and C1s lines and the qualitative and quantitative evaluations were performed in order to determine the surface composition and rationalize the chemical environment of the main constituent elements. For illustrating the alterations, the changing shapes of the O1s and C1s spectra are shown for the untreated GO, HT200, ASP200, and ASP200 samples in Figure 8.

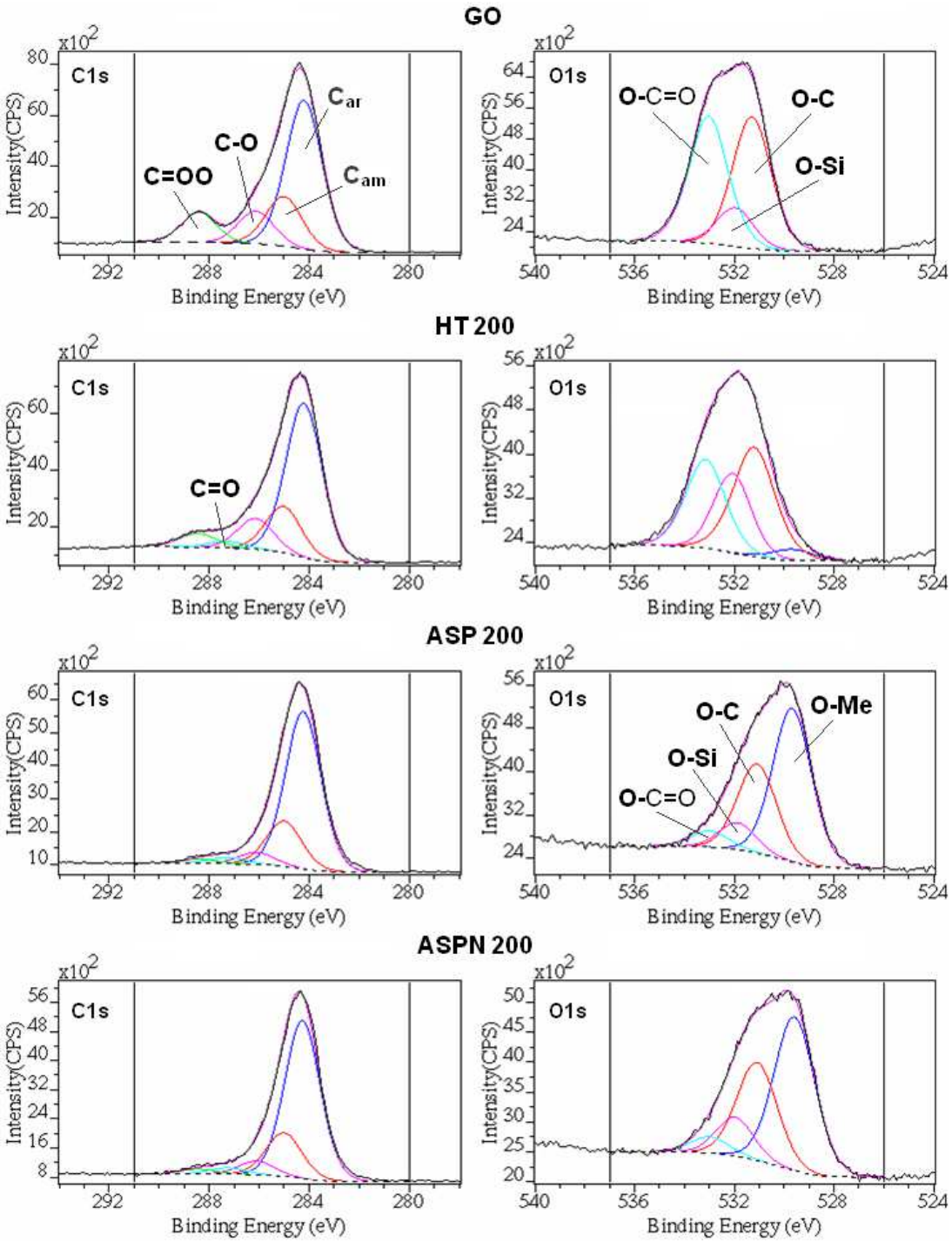

Figure 8. Comparison of high-resolution XP spectra of C1s and O1s lines of the as-cast GO and treated (HT200, ASP200, ASPN200) samples, showing complete coincidence of the sum of the component peaks with the experimental data. See details of chemical state assignation in the text

The high resolution spectra were decomposed into Gaussian-Lorenzian (70/30 ratio) components after Shirley type background removal. When synthesising the recorded line-shape with components, the principal guideline is to apply the minimum number of components.

Photoelectron lines of the main constituent elements, i.e., the O1s and C1s, were recorded by 0.1 eV steps, using non-monochromatic Mg $K\alpha_{1,2}$ (1253.6 eV) excitation and FAT analyser mode with 40 eV pass energy. At these settings the full width at half maximum (FWHM) of the Ag $3d_{5/2}$ peak is 1.54 eV. This value can be considered as the resolution for a single well-defined chemical state of a clean (metallic, i.e., conducting) sample. In our practice, this resolution has been rarely achieved for the components of oxide, nitride, carbide, DLC and CN_x samples. Due to the several slightly different bonding states caused predominantly by various "second neighbour" heteroatoms, somewhat larger FWHM was selected for the C1s (1.7±0.1 eV) and O1s (1.8±0.1 eV) components synthesising the measured peak envelope.

As seen in Fig. 8, both the carbon and oxygen can be found on the surface in various chemical states, represented by the synthetic component peaks. Assignment of these component peaks was made based on the large number of reliable literature data, compiled and published by us recently in [30] and their supplement.

Bonding of oxygen to carbon includes two O1s components: the high energy component at 533.0 eV is assigned to the single bonded oxygen in carboxylic group, nominated as O–O=C; the lower energy component at 531.1 eV marked as O–C, can be assigned equally to C–OH, epoxy type C–O–C or carbonyl C=O. The amount and position of O–Si (532.0 eV) and O–Me (529.7 eV) bonds were also determined. In the latter case, the metals (Me) are Fe, Cr and Mo.

Chemical states in the carbon network are represented by two C1s components, by the aromatic, graphene-like $C–C_{ar}$ at 284.3 eV and by the amorphous (destroyed structure) $C–C_{am}$ at 285.0 eV. The various carbon-oxygen bonds are the following: at 286.1 eV the C–O in C–OH, epoxy type C–O–C, at 287.3 eV

the carbonyl C=O and at 288.4 eV the carboxylic type C=OO. Nitrogen atoms are bonded to the carbon network as a broad peak centred at about 400 eV. N–O bonds were not detected.

The chemical composition of the elements C, O, N, Fe, Cr, Mo and Si, and of the O1s peak components and their assignment to different bonding states are given in Table 2. Regarding the oxygen, its total content was reduced appreciably already after heat treatment at 200 ºC from 20.8 to 17.4 atomic %. The reducing effect of the plasma treatments, however, could be judged neither by the change of the total oxygen content (column 1 in Table 2), nor by the expected increase of the total carbon content (column 2 of Table 2), because of the simultaneous build-up of the Fe, Cr, Mo doping elements, being in partially oxidized state. However, the amount of oxygen species bonded to carbon show a significant decrease: i.e., the O–C content from 9.0 in the untreated GO to 1–1.5 atomic % after plasma treatment. The O=C content also decreased from 9.2 to 6.6 atomic %. These oxygen losses (and their sum, O_C), can be the measure of the reduction of the GO samples together with the O_C/C ratios derived from those data (see last column in Table 2). After heat treatment at 200 ºC, the O_C/C ratio decreased already from 0.235 to 0.154, and it was further decreased by ASP and ASPN treatments.

Table 2. The overall chemical composition (atomic %) of the untreated and treated GO samples, the proportion of the oxygen chemical states and the O_C/C ratio

Sample	O	C	N	Si	Fe	Cr	Mo	O components				O_C/C
								O–Si	O–Me	O–C=O	O–C	
GO	20.8	77.2	0.0	2.0	0.0	0.0	0.0	2.6	0.0	9.2	9.0	0.235
HT200	17.4	79.3	1.0	2.2	0.0	0.0	0.0	4.3	0.0	7.4	5.7	0.154
ASP150	20.7	69.1	2.2	5.2	1.5	1.0	0.3	5.6	6.7	6.9	1.5	0.122
ASPN150	21.0	70.1	3.4	1.5	2.4	1.3	0.3	2.1	10.2	7.4	1.3	0.125
ASP200	19.6	71.4	2.3	1.3	2.9	2.0	0.3	1.7	10.6	6.2	1.1	0.102
ASPN200	21.1	69.0	2.1	2.1	3.3	2.0	0.3	2.4	10.8	6.8	1.1	0.115

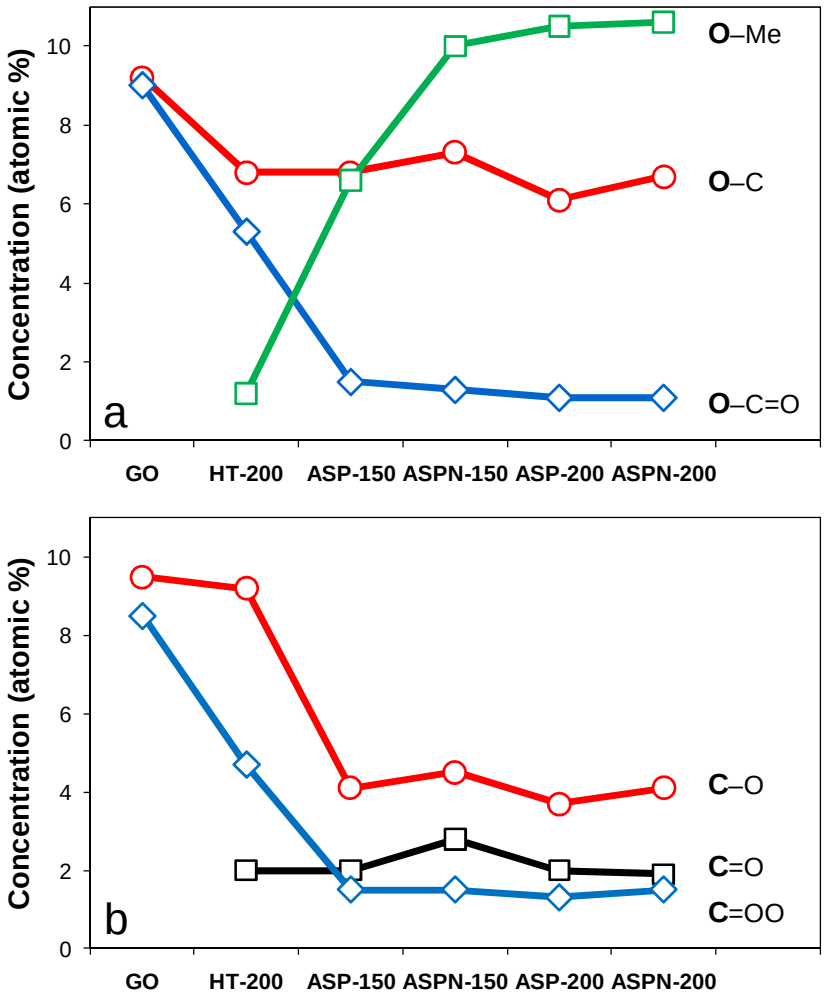

Figure 9. Change of the composition of the various oxygen (a) and carbon (b) chemical states for the untreated and treated samples as measured by XPS

The quantified data, calculated from the peak components in Fig. 8, are shown in Table 2 and in Fig. 9. The oxygen bonded to metals (O–Me, including O–Si) appeared in every plasma treated sample. Its quantity is proportional, to some extent, to the metallic components.

The changes in oxygen concentrations are different for the two chemical states (Fig. 9a). Data show that the single bonded carboxylic oxygen, **O**–C=O, is not stable, and its amount decreased most significantly due to the plasma treatments but partially also during the heat treatment. The other oxygen bonds, **O**–C (representing also C–**O**H, epoxy C–**O**–C, carbonyl C=**O**), seem to be more

stable than the carboxylic ones.

The quantity of carbon differently bonded to oxygen shows also major changes. The carboxylic carbon decreased most significantly, parallel to its **O**–C=O neighbours. The carbon bonded to oxygen as **C**–O, is relatively more stable than the previous one, as less altered in these treatments. A new chemical state of carbon, carbonyl type **C**=O, is developed due to all kind of treatments, most probably by the disruption of the carboxylic groups (Fig. 9b).

N was found in small quantity after different treatments, suggesting moderate doping through thermal annealing or AS plasma treatments. The residual N in the HT and ASP treated samples were believed to come from the residual air and from the chamber wall, contaminated during previous nitriding processes. The ASPN150 sample showed the higher N content than that of ASP150 sample, while the N contents were similar for the treatments at 200 ºC. This suggested that N-doping can be affected by not only the gas atmosphere but also the temperature. As mentioned above, the plasma surface interactions in active screen plasma treatments include combined mechanisms of sputtering and redeposition. The increased treating temperature can enhance the kinetic energy of particles in plasma, thus more nitrogen particles could be sputtered rather than deposited on the surface.

Metallic species such as Fe, Cr and Mo were found only in ASP and ASPN treated samples, as these originated from the plasma sputtering of the stainless steel mesh. The amount of Cr and Fe increased with the treating temperature (from 150 to 200 ºC) but the Mo content is constant. For example, after ASP and ASPN treatments Fe contents were increased from 1.5 to 2.9 atomic %, and from 2.4 to 3.3 atomic %, respectively. Meanwhile, the nitrogen-involved ASPN process is more effective than the nitrogen-free ASP process in increasing the content of Fe and Cr. For instance, the content of Fe was increased from 1.5 to 2.4 atomic %, and from 2.9 to 3.3 atomic %, respectively,

for the 150 ºC and 200 ºC processes. The deposition process of the metallic components involves the sputtering which can be intensified by increasing both the energy and the mass of the particles.[38] This finding inspired that different elements can be doped by properly selecting the material of the active screen, and their contents may be tuneable by altering the plasma energy and process conditions, such as the temperature, bias, time, distance between the mesh and samples.

3.7 Relationship between property and chemical changes

As have been reported in Sections 3.2 and 3.3, active screen plasma treatments including ASP and ASPN can effectively reduce GO as evidenced by the decreased electrical conductivity (Fig. 4) and transmission of UV-visible light (Fig. 3). The change of such macroscopic physical properties by active screen plasma treatments could be explained by the atomic scale chemical changes detected by XPS. As shown in Table 2, the O_c/C ratio- the measure of the reduction GO samples can be decreased from 0.235 for the untreated GO to 0.154 by thermal annealing at 200 °C (HT200) and active screen plasma treatment at the same temperature can further reduce it to 0.115 and 0.102 by ASPN200 and ASP200, respectively.

It is of scientific interest to note that ASP is more effective than ASPN in reducing GO as evidenced by the lower O_c/C ratio (Table 2) and transmission (Fig. 3) of ASP treated GO than ASPN treated one. However, the electrical resistance results in Figure 4 show that although both ASPN and ASP treatments can dramatically reduce the electrical resistance of GO, the former (ASPN) is much more effective than the latter (ASP) especially when treated at a relatively low temperature of 150 °C. Obviously, this observation could not be explained by the O_c/C ratio alone since the O_c/C ratio of ASP is lower than that for ASPN (Table 2).

This seemingly contradicting observation could be interpreted by the fact that ASPN is more effective than ASP in multi-element doping of GO. As shown in Table 2, when treated at the same temperature of 150°C, more Fe and Cr were detected from the ASPN150 treated GO surface than from the ASP150 treated one. It is known that the sputtering of metals can be intensified by increasing the mass of the particles.[38] Nitrogen is much heavier than hydrogen and hence more metallic atoms will be sputtered out from the austenitic stainless steel screen and deposited on the surface of GO. Consequently, a GO surface with a lower electrical resistance can be generated by ASPN150 than by ASP150, which shows one of the advantages of multi-element doping.

4. Conclusions

In summary, a transparent GO layer on a nonconductive PET substrate has been successfully reduced by active screen plasma treatments in H_2 (ASP) and in a gas mixture of H_2 and N_2 (ASPN) at moderately high temperatures (100-200 ºC). The plasma treatments have led to a greater extent of reduction of GO as compared to the thermal annealing at the same temperature. The active screen plasma treatments in H_2 (ASP) can reduce the GO more effectively than the active screen plasma treatments in a gas mixture of 25%N_2 + 75%H_2 (ASPN).

Detailed XPS analyses have revealed that the carboxylic O–C is not stable, and its amount can be reduced by thermal annealing and more effectively by active screen plasma treatments. A new chemical state of carbon, carbonyl type **C**=O, is developed most probably from the decomposed carboxyl groups due to the treatments.

XPS results have proved that simultaneous doping of graphene oxide both with N from the gas supply and with metallic species of Fe, Cr and Mo from the active screen can be performed at the same time. It has been demonstrated that the ASPN treatment (using both N_2 and H_2) is more effective than the ASP treatment (using H_2 along) in increasing the electrical conductivity of graphene

oxide. This is mainly because nitrogen is much heavier than hydrogen and hence more metallic atoms will be sputtered out from the steel screen and then deposited on the surface of GO.

The extent of doping can be tuned by applying different process conditions, such as the gas composition, temperature, bias, time, distance between the sample surface and the mesh. This can open a door for doping graphene related materials, such as non-conductive graphene oxide, conductive graphene and reduced graphene oxide, etc. in various applications such as biosensors.

Acknowledgements

The authors gratefully acknowledge the financial support from the NSFC (#11204031 and #11472080), the NSF of Jiangsu Province of China (#BK20141336) and Jiangsu key laboratory of advanced metallic materials (BM2007204). This work was also sponsored by the Hungarian National Scientific Research Fund (OTKA) through the project No. K-109558. One of the authors (QJ) appreciates a PhD studentship jointly provided by Chinese Scholars Council and by the University of Birmingham.

References:

[1] Novoselov KS, Fal Prime Ko VI, Colombo L, Gellert PR, Schwab MG, Kim K. A roadmap for graphene. NATURE. 2012;490(7419):192-200.

[2] Lee Y, Ahn J. GRAPHENE-BASED TRANSPARENT CONDUCTIVE FILMS. NANO. 2013;8(13300013).

[3] Li XS, Cai WW, An JH, Kim S, Nah J, Yang DX, et al. Large-Area Synthesis of High-Quality and Uniform Graphene Films on Copper Foils. SCIENCE. 2009;324(5932):1312.

[4] Park S, Ruoff RS. Chemical methods for the production of graphenes. NAT NANOTECHNOL. 2009;4(4):217-24.

[5] Zhu Y, Murali S, Cai W, Li X, Suk JW, Potts JR, et al. Graphene and Graphene Oxide: Synthesis, Properties, and Applications. ADV MATER. 2010;22(35):3906-24.

[6] Go·mez-Navarro C, Meyer JC, Sundaram RS, Chuvilin A, Kurasch S, Burghard M, et al. Atomic Structure of Reduced Graphene Oxide. NANO LETT. 2010 2010-04-14;10(4):1144-8.

[7] Dreyer DR, Park S, Bielawski CW, Ruoff RS. The chemistry of graphene oxide. CHEM SOC REV. 2010;39(1):228-40.

[8] Pei SF, Cheng HM. The reduction of graphene oxide. CARBON. 2012;50(9):3210-28.

[9] Stankovich S, Dikin DA, Piner RD, Kohlhaas KA, Kleinhammes A, Jia Y, et al. Synthesis of

graphene-based nanosheets via chemical reduction of exfoliated graphite oxide. CARBON. 2007;45(7):1558-65.

[10] Chen CM, Huang JQ, Zhang Q, Gong WZ, Yang QH, Wang MZ, et al. Annealing a graphene oxide film to produce a free standing high conductive graphene film. CARBON. 2012;50(2):659-67.

[11] Janowska I, Chizari K, Ersen O, Zafeiratos S, Soubane D, Da Costa V, et al. Microwave synthesis of large few-layer graphene sheets in aqueous solution of ammonia. NANO RES. 2010;3(2):126-37.

[12] Zhang H, Lv X, Li Y, Wang Y, Li J. P25-Graphene Composite as a High Performance Photocatalyst. ACS NANO. 2010;4(1):380-6.

[13] Ramesha GK, Sampath S. Electrochemical Reduction of Oriented Graphene Oxide Films: An in Situ Raman Spectroelectrochemical Study. J PHYS CHEM C. 2009 1990-05-01;113(19):7985-9.

[14] Wang H, Robinson JT, Li X, Dai H. Solvothermal reduction of chemically exfoliated graphene sheets. J AM CHEM SOC. 2009;131(29):9910-1.

[15] Gao XF, Jang J, Nagase S. Hydrazine and Thermal Reduction of Graphene Oxide: Reaction Mechanisms, Product Structures, and Reaction Design. J PHYS CHEM C. 2010;114(2):832-42.

[16] Ren PG, Yan DX, Ji X, Chen T, Li ZM. Temperature dependence of graphene oxide reduced by hydrazine hydrate. NANOTECHNOLOGY. 2011;22(0557055).

[17] Obata S, Tanaka H, Saiki K. Electrical and spectroscopic investigations on the reduction mechanism of graphene oxide. CARBON. 2013;55:126-32.

[18] Shin HJ, Kim KK, Benayad A, Yoon SM, Park HK, Jung IS, et al. Efficient Reduction of Graphite Oxide by Sodium Borohydrilde and Its Effect on Electrical Conductance. ADV FUNCT MATER. 2009 1990-06-01;19(12):1987-92.

[19] Fan XB, Peng WC, Li Y, Li XY, Wang SL, Zhang GL, et al. Deoxygenation of Exfoliated Graphite Oxide under Alkaline Conditions: A Green Route to Graphene Preparation. ADV MATER. 2008;20(23):4490-3.

[20] Gao J, Liu F, Liu YL, Ma N, Wang ZQ, Zhang X. Environment-Friendly Method To Produce Graphene That Employs Vitamin C and Amino Acid. CHEM MATER. 2010;22(7):2213-8.

[21] Fernandez-Merino MJ, Guardia L, Paredes JI, Villar-Rodil S, Solis-Fernandez P, Martinez-Alonso A, et al. Vitamin C Is an Ideal Substitute for Hydrazine in the Reduction of Graphene Oxide Suspensions. J PHYS CHEM C. 2010;114(14):6426-32.

[22] Pei SF, Zhao JP, Du JH, Ren WC, Cheng HM. Direct reduction of graphene oxide films into highly conductive and flexible graphene films by hydrohalic acids. CARBON. 2010;48(15):4466-74.

[23] Jung I, Field DA, Clark NJ, Zhu YW, Yang DX, Piner RD, et al. Reduction Kinetics of Graphene Oxide Determined by Electrical Transport Measurements and Temperature Programmed Desorption. J PHYS CHEM C. 2009;113(43):18480-6.

[24] Yang D, Velamakanni A, Bozoklu G, Park S, Stoller M, Piner RD, et al. Chemical analysis of graphene oxide films after heat and chemical treatments by X-ray photoelectron and Micro-Raman spectroscopy. CARBON. 2009;47(1):145-52.

[25] Kang H, Kulkarni A, Stankovich S, Ruoff RS, Baik S. Restoring electrical conductivity of dielectrophoretically assembled graphite oxide sheets by thermal and chemical reduction techniques. CARBON. 2009;47(6):1520-5.

[26] Kim CJ, Khan W, Park SY. Structural evolution of graphite oxide during heat treatment. CHEM PHYS LETT. 2011;511(1-3):110-5.

[27] Wang Y, Shao Y, Matson DW, Li J, Lin Y. Nitrogen-Doped Graphene and Its Application in Electrochemical Biosensing. ACS NANO. 2010 2010-04-27;4(4):1790-8.

[28] Kumar NA, Nolan H, McEvoy N, Rezvani E, Doyle RL, Lyons MEG, et al. Plasma-assisted simultaneous reduction and nitrogen doping of graphene oxide nanosheets. J MATER CHEM A. 2013;1(14):4431.

[29] Wang HB, Maiyalagan T, Wang X. Review on Recent Progress in Nitrogen-Doped Graphene: Synthesis, Characterization, and Its Potential Applications. ACS CATAL. 2012;2(5):781-94.

[30] Bertóti I, Mohai M, László K. Surface modification of graphene and graphite by nitrogen plasma: Determination of chemical state alterations and assignments by quantitative X-ray photoelectron spectroscopy. CARBON. 2015;84:185-96.

[31] Shao Y, Zhang S, Engelhard MH, Li G, Shao G, Wang Y, et al. Nitrogen-doped graphene and its electrochemical applications. Journal of Materials Chemistry. 2010;20(35):7491.

[32] Imran Jafri R, Rajalakshmi N, Ramaprabhu S. Nitrogen doped graphene nanoplatelets as catalyst support for oxygen reduction reaction in proton exchange membrane fuel cell. Journal of Materials Chemistry. 2010 2010-01-01;20(34):7114-7.

[33] Li CX, Bell T. Potential of plasma nitriding of polymer for improved hardness and wear resistance. J MATER PROCESS TECH. 2005;168(2):219-24.

[34] Fu X, Jenkins MJ, Sun GM, Bertoti I, Dong HS. Characterization of active screen plasma modified polyurethane surfaces. SURF COAT TECH. 2012;206(23):4799-807.

[35] Chen J, Li XY, Ji R, Khan R, Fuentes G. Nanomechanical properties of duplex treated 42CrMo4 steel. SURF ENG. 2013;29(6):462-7.

[36] Hedayati MK, Mahboubi F, Nickchi T. Comparison of conventional and active screen plasma nitriding of hard chromium electroplated steel. VACUUM. 2009;83(8):1123-8.

[37] Fu X, Sammons RL, Bertoti I, Jenkins MJ, Dong HS. Active screen plasma surface modification of polycaprolactone to improve cell attachment. J BIOMED MATER RES B. 2012;100B(2):314-20.

[38] Gallo SC, Dong HS. On the fundamental mechanisms of active screen plasma nitriding. VACUUM. 2009;84(2):321-5.

[39] Marcano DC, Kosynkin DV, Berlin JM, Sinitskii A, Sun ZZ, Slesarev A, et al. Improved Synthesis of Graphene Oxide. ACS NANO. 2010;4(8):4806-14.

[40] Diaz J, Paolicelli G, Ferrer S, Comin F. Separation of the sp3 and sp2 components in the C1s photoemission spectra of amorphous carbon films. Phys Rev B Condens Matter. 1996 1996-09-15;54(11):8064-9.

[41] Haerle R, Riedo E, Pasquarello A, Baldereschi A. sp2/sp3 hybridization ratio in amorphous carbon from C 1s core-level shifts: X-ray photoelectron spectroscopy and first-principles calculation. Physical review. B, Condensed matter. 2001;65:45101.

[42] Mohai M, Bertóti I. Calculation of layer thickness on nanotube surfaces from XPS intensity data. SURF INTERFACE ANAL. 2012;44(8):1130-4.

[43] Bertóti I, Mohai I, Mohai M, Szépvölgyi J. Surface modification of multi-wall carbon nanotubes by nitrogen attachment. DIAM RELAT MATER. 2011;20(7):965-8.

[44] Wagner CD, Riggs WM, Davis LE, Moulder JF, Muilenberg GT. Handbook of X-ray photoelectron spectroscopy: Perkin-Elmer Eden Prairie, MN 1970.

[45] Moulder JF, Chastain J, King RC. Handbook of X-ray photoelectron spectroscopy: a reference book of standard spectra for identification and interpretation of XPS data: Perkin-Elmer Eden Prairie, MN 1992.

[46] Beamson G, Briggs D. High resolution XPS of organic polymers: The Scienta ESCA300 Database. Chichester: John Wiley & Sons 1992.

[47] Technology NIOS. NIST X-ray Photoelectron Spectroscopy Database. Version 4.1 ed: Gaithersburg 2012.

[48] Mohai M, Bertoti I. Calculation of overlayer thickness on curved surfaces based on XPS intensities. SURF INTERFACE ANAL. 2004;36(8):805-8.

[49] Mohai M. XPS MultiQuant: multimodel XPS quantification software. SURF INTERFACE ANAL. 2004;36(8):828-32.

[50] Evans S, Pritchard RG, Thomas JM. Relative differential subshell photoionisation cross-sections (MgK α) from lithium to uranium. J ELECTRON SPECTROSC. 1978;14(5):341-58.

[51] Reilman RF, Msezane A, Manson ST. Relative intensities in photoelectron spectroscopy of atoms and molecules. J ELECTRON SPECTROSC. 1976;8(5):389-94.

[52] Wilson NR, Pandey PA, Beanland R, Young RJ, Kinloch IA, Gong L, et al. Graphene Oxide: Structural Analysis and Application as a Highly Transparent Support for Electron Microscopy. ACS NANO. 2009;3(9):2547-56.

[53] Schniepp HC, Li JL, McAllister MJ, Sai H, Herrera-Alonso M, Adamson DH, et al. Functionalized single graphene sheets derived from splitting graphite oxide. J PHYS CHEM B. 2006 1990-05-01;110(17):8535-9.

[54] Dimiev AM, Tour JM. Mechanism of Graphene Oxide Formation. ACS NANO. 2014;8(3):3060-8.

[55] Biroju RK, Giri PK. Defect Enhanced Efficient Physical Functionalization of Graphene with Gold Nanoparticles Probed by Resonance Raman Spectroscopy. J PHYS CHEM C. 2014 2014-06-26;118(25):13833-43.

[56] Ferrari AC, Meyer JC, Scardaci V, Casiraghi C, Lazzeri M, Mauri F, et al. Raman spectrum of graphene and graphene layers. PHYS REV LETT. 2006;97(18740118).

[57] Kudin KN, Ozbas B, Schniepp HC, Prud'Homme RK, Aksay IA, Car R. Raman spectra of graphite oxide and functionalized graphene sheets. NANO LETT. 2008;8(1):36-41.